Estimates of North Atlantic Ventilation and Mode Water Formation for Winters 2002-2006

David S. Trossman
School of Oceanography, University of Washington, Seattle, WA

LuAnne Thompson
School of Oceanography, University of Washington, Seattle, WA

Kathryn A. Kelly
Applied Physics Laboratory, University of Washington, Seattle, WA

Young-Oh Kwon
Woods Hole Oceanographic Institution, Woods Hole, MA

In prep for *Journal of Physical Oceanography*, May 16, 2009

Short title: NORTH ATLANTIC VENTILATION

Abstract.

Lagrangian estimates for ventilation rates in the Gulf Stream Extension using Argo and World Ocean Circulation Experiment (WOCE)/Atlantic Climate and Circulation Experiment (ACCE) float data, scatterometer (QuikSCAT) wind stress satellite observations, and altimetric (Aviso) sea surface height (SSH) satellite observations from 2002 to 2006 are presented. Satellite winds and estimates of surface geostrophic currents allow the inclusion of the effects of currents on wind stress as well as their impact on the Ekman pumping. The presence of large surface geostrophic currents decrease the total Ekman pumping, contributing up to 20 % where the Gulf Stream makes its two sharpest turns, and increases the total Ekman pumping by 10 % or less everywhere else. The ageostrophic currents may be as large as 15 % of the geostrophic currents, but only in proximity of the Gulf Stream.

Using currents and mixed-layer depths (MLDs) that are either climatological or vary from year to year, obducted water tends to originate along the Gulf Stream, while subducted water tends to originate to its south. However, using time-varying MLDs for each year, subduction varies significantly, sometimes oppositely from obduction. Eighteen Degree Water (EDW) subducts in different locations and is distributed differently each year, but tends to be located in the Sargasso Sea. Vertical pumping is the only dominant factor in ventilation closer to the coast where MLDs are shallower and lighter parcels are subducted. Vertical pumping contributes up to 20 % of the several hundreds of ventilated meters per year around the Gulf Stream and less elsewhere. Using a temperature-based criterion or a density-based criterion for estimating the MLDs, especially along the coasts and north of 45^oN, obduction estimates differ by up to 25 %. The horizontal and temporal structure of the MLDs is the primary factor that controls the tens of Sverdrups of ventilation (and a few Sverdrups of EDW subduction).

1. Introduction

The upper ocean that separates the atmosphere and the permanent thermocline consists of an Ekman layer, a mixed layer, and a seasonal thermocline. Water parcels gain their identities in the mixed layer and keep their identities to a great extent in the thermocline. In order to understand climate variability and water mass formation, it is important to know about water mass exchange rates between the surface and the permanent thermocline. The ocean can exchange properties such as heat with the atmosphere and may store these properties for decades or longer through transfer to the thermocline (*Williams*, 2001).

Subduction is the mass flux from the seasonal thermocline into the permanent thermocline. Obduction is the (irreversible) mass flux into the seasonal thermocline from the permanent thermocline. These processes may also be referred to as ventilation. The top of the seasonal thermocline is defined as the shallowest depth at which the mixed layer's base is mixed within a given year. The top of the permanent thermocline is defined as the deepest mixed layer depth within a given year. Seasonally, the entire column of water down to the base of the seasonal thermocline has been mixed, but may not be mixing.

Because temperature and salinity are not conserved when water parcels are mixed, the top of the permanent thermocline is the relevant boundary when considering conservation of physical properties of water parcels. It was believed by *Iselin* (1939) that Ekman pumping in the late winter (March) forced water to cross the base of the wind-generated Ekman layer and flow along isopycnals thereafter. *Stommel* (1979) hypothesized that taking all mixed layer parameters from late winter can bypass the complication of the seasonal cycle and thus the seasonal thermocline can be ignored. Climatological estimates using Stommel's hypothesis assume water parcels subducted from the summer mixed layer are generally re-entrained as the mixed layer deepens the following winter. This is usually referred to as Stommel's mixed layer demon.

In addition to the sign difference, obduction and subduction are different in three ways, according to *Qiu and Huang* (1995): (1) Different physical processes govern them.

Temperature and salinity properties, as determined by the mixed layer processes, will be carried by the subducted water to the permanent thermocline. On the other hand, water loses its identity via convective mixing when water is obducted. (2) Subduction and obduction have different annual cycles. Subduction occurs after late winter when the mixed layer restratifies and obduction occurs between late fall and early winter when the mixed layer is deepening. (3) A mean annual subduction rate is an estimate of how much water enters the permanent thermocline, while a mean annual obduction rate is an estimate of how much water comes from the permanent thermocline.

Local maxima in the subduction of water occur where there are 'mode' waters, where the water column is nearly vertically homogeneous in density. The mode waters of interest here are also characterized by temperatures between 17 and 19^{o}C (*Worthington*, 1959). Because of this property, its alternate name is Eighteen Degree Water (EDW). This well-defined water mass is important for the storage of heat and chemical constituents in the North Atlantic. While surface heat fluxes largely determine the sea surface temperature (SST) variability in most of the World Ocean, heat transport by geostrophic flow makes as comparable contribution as surface heat fluxes in the northwestern North Atlantic (*Dong and Kelly*, 2004). *Dong and Kelly* (2004) have also shown that the interannual heat transport is primarily driven by geostrophic currents, not by Ekman currents.

EDW is a link between the ocean and atmosphere. Production of EDW is believed to be connected to the North Atlantic Oscillation (NAO), sea surface density anomalies near the Gulf Stream, and deep water formation in the North Atlantic subpolar regions (*Curry and McCartney*, 2001). The EDW typically forms just south of the Gulf Stream, where it cools (to the lower end of the 17 to 19^{o}C range) and recirculates. Years with greater EDW production tend to have EDW closer to 17^{o}C while years with lower production have warmer EDW, as the EDW mixes with warmer recirculating water (*Kwon*, 2003). EDW is also an important component of the near surface overturning circulation and for transferring biogeochemical properties between the near-surface and the ocean interior since EDW is depleted of nutrients

and rich in carbon content (*Palter et al.*, 2005).

Joyce et al. (2000) found that the Gulf Stream (northern latitude) position, NAO index, and EDW potential vorticity (or lack of EDW production) are highly correlated with one another with a zero lag time. The EDW potential vorticity is also highly correlated with large-scale atmospheric forcing. Hence, three factors have been thought to influence EDW variability: (1) Gulf Stream position, (2) ocean-atmosphere heat fluxes, and (3) temperature and salinity anomaly advection. However, *Dong et al.* (2007) has found that both the oceanic advective convergence and the product of heat fluxes and the area of the outcropping 17 to 19^{o}C isotherms, not variability of surface heat flux, play the most important roles in EDW variability. The oceanic advective convergence indicates the importance of (1) and (3) while the area of the outcropping 17 to 19^{o}C isotherms indicates the importance of preconditioning. Since the NAO affects the SSTs, a link between the NAO and EDW may be drawn if it may be shown that the SSTs affect EDW volume.

Kwon and Riser (2004) have shown that EDW volume reaches its annual peak in the winter. Using profile estimates, they show that the formation rate of EDW is on the order of $4 - 5$ Sv from profile estimates, as opposed to the $15 - 20$ Sv *Speer and Tziperman* (1992) estimated from air-sea fluxes using the *Walin* (1982) formulation. The *Walin* (1982) formulation diagnoses the EDW formation rates by using diabatic forcings as a function of outcropping isopycnals. No circulation or mixing is included so mixing of density within the interior is ignored. *Nurser et al.* (1999) found both deepening of the Winter mixed layer and lateral mixing within the mixed layer (including entrained denser waters into lighter ones) to be potentially significant at mid-latitudes, albeit less significant than mixing in sustained upwelling regions in the tropics. The discrepancy between the estimates of *Kwon and Riser* (2004) and *Speer and Tziperman* (1992) may be caused by an error in the *Walin* (1982) formulation or inaccurate air-sea fluxes, but most probably can be accounted for by the lateral mixing, or eddy processes, that result in lateral transport in the mixed layer near the Gulf Stream. These processes have patchy spatial distributions to which bulk parameters may not

do justice.

Here we build on the work of *Qiu and Huang* (1995) who made subduction rate estimates for the North Atlantic (and Pacific) with climatological estimates for MLDs, climatological estimates for currents, and *Hellerman and Rosenstein* (1983) wind stress data (which has been noted to overestimate the wind stress by 30 % (*Harrison*, 1989)). We recalculate Ekman pumping, as *Xie* (2004) did with QuikSCAT wind stress data from 1999 to 2003, but including the impact of upper ocean geostrophic currents on Ekman velocities. We include winds, currents, observationally-derived MLDs, and vertical shear to calculate (EDW) ventilation rates and compare with previous estimates. Section 2 describes the data we use in our Ekman pumping and (EDW) ventilation rate estimates. We end with results in Section 3 before summarizing.

2. Data and Methods

Due to recent realizations of satellite and profiler systems, we are not only able to investigate inter-annual variability in a few selected locations, but intra-annual variability across the Gulf Stream and Sargasso Sea. QuikSCAT winds are available daily from July 1999 and mapped as in *Kelly et al.* (1999), Aviso SSHs are available weekly from October 1992, Argo temperatures and salinities are available every ten days from the year 2000, and WOCE/ACCE MLDs and temperatures are from 1997 through 2003. WOA (World Ocean Atlas of 1994) temperature and salinity climatologies are available for each month of the year. Our data is summarized in Table 1.

2.1. Surface Currents

The Aviso SSH product, on a $1/3^o \times 1/3^o$ grid, also includes error maps which indicate significant errors located between the tracks of TOPEX/Poseidon and Jason-1. Because of these errors, surface geostrophic flow calculated from the SSH anomalies show signals that reflect the satellite track patterns. The anomalies have high frequency

noise and coverage errors in them while the mean does not, as the mean was derived from historical and hydrographic float (surface) data following *Singh and Kelly* (1997) (http://kelly.apl.washington.edu/projects/meanssh.html). Because more structural detail would be lost if the sum of the anomalies and mean SSHs is filtered, we first filter the anomalies and then add on the mean SSHs (not filtered by us). We use spatial low-pass filtering on the SSH anomalies data after temporally averaging over three week blocks of time. We use a half-power of six longitudinally (between 80 and 30^oW) and a half-power of five latitudinally (between 20 and 55^oN), low-pass filtering once in each direction with a Butterworth filter. In regions where the errors are greater than their corresponding SSH anomalies, we assume that these SSH anomalies are zero, which are typically when errors exceeded 20 cm. The only places with greater errors are along the coast (with errors sometimes as high as 50 cm). We set our final SSH to be the sum of these low-passed anomalies and the mean Aviso SSH.

The resulting currents are derived from the geostrophic relationships

$$u_g = -\frac{g}{f}\frac{\partial \eta}{\partial y} \tag{1}$$

$$v_g = \frac{g}{f}\frac{\partial \eta}{\partial x}, \tag{2}$$

where $g = 9.81$ m/s^2, f is the Coriolis parameter which we allow to vary with latitude, and η is the SSH. These currents do not show a track pattern. Additional filtering was applied to mask over the jump between land and nonzero currents. If the difference between the currents between two grid points was $.25$ m/s or larger, then the currents from that longitude to the west-most grid point and within a box of three latitudinal grid points are set to zero. The mean annual geostrophic surface currents' structure maps out the Gulf Stream (left-hand side of Fig. 1). The objective map gives smaller SSH anomalies in regions of larger errors, which in turn gives smaller current speeds.

2.2. Shear

To obtain the vertical structure of the currents, we low-pass filter the potential densities averaged monthly from Jan. 2002 to Dec. 2006 using the same procedure as was used in low-pass filtering the SSH: once with a half-power of six longitudinally (between 80 and 30^oW) and a half-power of five latitudinally (between 20 and 55^oN). We find these potential densities using WOA (T,S) data when the errors associated with objectively mapped Argo (T,S) data exceed 50 m as calculated according to the objective mapping method of *Le Traon* (1990). Then we use the thermal wind equations,

$$\frac{\partial u_g}{\partial z} = \frac{g}{f\rho_o}\frac{\partial \rho_\theta}{\partial y} \tag{3}$$

$$\frac{\partial v_g}{\partial z} = -\frac{g}{f\rho_o}\frac{\partial \rho_\theta}{\partial x}, \tag{4}$$

where ρ_θ is the potential density and ρ_o is the mean density over our domain.

We grid these current shears with a fifty meter vertical resolution, vertically integrate, and use the Aviso surface currents from the previous section as a reference. The ratio of the currents at some depth to currents at the surface is capped at one, filled with the spatially averaged ratios for this depth if greater than one (which occurs at less than 10 % of grid points). These currents are low-pass filtered once in both horizontal directions with a half-power of four. Lastly, we fit logarithmic curves to the profiles of these ratios and low-pass filter with a half-power of four again for a small shear profile.

2.3. Ekman Pumping

One way water parcels may obduct or subduct is by vertical advection, or vertical pumping through Ekman currents (Appendix). Ekman pumping is defined by $-w_e \equiv -\vec{\nabla}\cdot\vec{U_e}$, as a convergence of Ekman transports, $\vec{U_e}$, which leads to a downward motion. An upward motion results from positive Ekman suction, w_e. Usually, the Ekman transports are

approximated with wind momentum input uncoupled from currents:

$$U_e = \frac{1}{\rho}\frac{\tau^y}{f} \quad (5)$$

$$V_e = -\frac{1}{\rho}\frac{\tau^x}{f}, \quad (6)$$

here, called the simple Ekman balance (Appendix). This analytical approximation, which *Qiu and Huang* (1995) and *Xie* (2004) have used for w_e, is valid in most regions, but the assumptions fail in the Gulf Stream. If surface geostrophic currents are strong then the vertically averaged flow in the Ekman layer satisfies (Appendix):

$$\frac{\partial U_e}{\partial t} + U_e\frac{\partial u_g}{\partial x} + u_g\frac{\partial U_e}{\partial x} + V_e\frac{\partial u_g}{\partial y} + v_g\frac{\partial U_e}{\partial y} - fV_e = \frac{\tau^x}{\rho} - \tau_{damp}U_e \quad (7)$$

$$\frac{\partial V_e}{\partial t} + U_e\frac{\partial v_g}{\partial x} + u_g\frac{\partial V_e}{\partial x} + V_e\frac{\partial v_g}{\partial y} + v_g\frac{\partial V_e}{\partial y} + fU_e = \frac{\tau^y}{\rho} - \tau_{damp}V_e. \quad (8)$$

We have used the approximation of *Qiu and Huang* (1995) and *Xie* (2004) for a first guess to the Ekman pumping. We also impose the simple Ekman balance at the coasts. Such regions serve as boundaries to the regions in which the *Qiu and Huang* (1995) approximation is not valid and help define a well-posed problem. To numerically solve for a converged solution, we have applied a time difference method with time steps, $\Delta t = 1/2$ hr. The geostrophic currents are held fixed for each week of Aviso SSH data and QuickScat wind data. To find the Ekman solutions, we time step, including accelerations as well as damping terms, $\tau_{damp}U_e$ and $\tau_{damp}V_e$. The damping factor, τ_{damp}, should be short relative to the temporal resolution of our data, a week, and long relative to the time steps, Δt. Running for $2/\tau_{damp}$ days, the solution reaches steady state. This yields the Ekman currents, and from this, we calculate w_e. The root-mean-squared differences between using $\tau_{damp} = 1/1$ day^{-1} and $\tau_{damp} = 1/1.675$ day^{-1} for u_e, v_e, and w_e, respectively are 0.0020 +/- 0.0014 m/s, 0.0016 +/- 0.0009 m/s, and 2.55×10^{-7} +/- 1.19×10^{-7} m/s. The solution does depend on τ_{damp}, but we choose $\tau_{damp} = 1/1.675$ day^{-1} to ensure enough time for the Ekman layer to set up.

2.4. Subduction Rate Approximation

Subduction is defined as positive when fluid descends through the thermocline, so that subduction is positive when w_e is negative. This can be seen in the expression for approximate mean annual subduction rates (*Marshall et al.*, 1993), (*Qiu and Huang*, 1995):

$$S_{ann} = -\overline{(w_e - \frac{\beta}{f}\int_{-\delta_e}^{0} v_g dz)} + \frac{1}{\tau}(h_{m,0} - h_{m,1}). \tag{9}$$

Here, τ is one year and $h_{m,0}$ and $h_{m,1}$ are the March MLDs for the year in which we want to compute the mean subduction rate and the year after that, respectively. The first term represents vertical pumping and the second term represents lateral induction. Average rates of obduction may be computed similarly but with MLD information from one year and the year previous. Over a period, τ, an average subduction rate may be computed via:

$$S_{avg} = -\frac{1}{\tau}\int_{t_0}^{t_1} w_{tr} dt - \frac{1}{\tau}\int_{t_0}^{t_1}(\frac{\partial h_m}{\partial t} + u_{tr}\frac{\partial h_m}{\partial x} + v_{tr}\frac{\partial h_m}{\partial y})dt \tag{10}$$

where t_0 and t_1 are the initial and final times (functions of space and year in our parcel tracking model to be discussed later), $\tau = t_1 - t_0$, w_{tr} and (u_{tr}, v_{tr}) are the vertical and horizontal velocities at the base of the mixed layer, h_m is the maximum depth of the mixed layer in the given year, and the $\partial h_m/\partial t$ term averages to zero over a sufficiently long τ (*Qiu and Huang*, 1995).

2.5. MLDs

Water parcels may also obduct or subduct by movement of the MLDs relative to a water parcel that allows the MLD to entrain (obduct) or detrain (subduct) this parcel (9). The MLDs are calculated using Argo and WOCE/ACCE data. When available, we use adjusted temperatures and salinities and only measurements with quality ‘1‘ ratings (http://www.coriolis.eu.org/cdc/argo_rfc.htm). The floats with World Meteorological Organization (WMO) identification number 852 from 2004 onward have been excluded due to a non-constant cold bias discovered in February of 2007 (http://argo.jcommops.org). These

floats were fairly uniformly distributed in the North Atlantic, leaving coverage as shown in Figure 2. Thus, while we expect the MLDs to be biased low including these data and to be higher excluding these data, the MLDs should be better with their exclusion.

We use the shallowest pressures at which the criterion, $\Delta T > 0.3^o$C, is satisfied unless stated otherwise. Here, ΔT is the difference between the surface temperature and the *in situ* temperature at some depth. Alternatively, $\Delta\rho_\theta > 0.125$ kg/m^3 may be used as a criterion where $\Delta\rho_\theta$ is the difference between the surface density and the potential density at some depth. Using the $\Delta T > 0.3$ criterion to estimate the MLDs yields results that look qualitatively different from those obtained using $\Delta\rho_\theta > 0.125$ as a criterion along the coasts and north of 45^oN. Despite how we should be using the $\Delta\rho_\theta > 0.125$ criterion, our WOCE/ACCE data lacks salinity so we settle with the $\Delta T > 0.3$ criterion.

For each grid point, we calculate a simple two-sample t-statistic with

$$t = (\overline{MLD_T} - \overline{MLD_{\rho_\theta}})\sqrt{(\frac{\sigma_T^2}{n_T} + \frac{\sigma_{\rho_\theta}^2}{n_{\rho_\theta}})^{-1}}, \tag{11}$$

with degrees of freedom

$$df = (\frac{\sigma_T^2}{n_T} + \frac{\sigma_{\rho_\theta}^2}{n_{\rho_\theta}})^2\sqrt{(\frac{1}{n_T - 1}(\frac{\sigma_T^2}{n_T})^2 + \frac{1}{n_{\rho_\theta} - 1}(\frac{\sigma_{\rho_\theta}^2}{n_{\rho_\theta}})^2)^{-2}}, \tag{12}$$

σ^2 representing the sample temporal variance where the MLDs are not zero, $n = 48$ representing the number of months in our sample, T subscripts corresponding to estimates derived from the $\Delta T > 0.3$ criterion, and ρ_θ subscripts corresponding to estimates derived from the $\Delta\rho_\theta > 0.125$ criterion (*Snedecor and Cochran*, 1989). We reject the null hypothesis that the (averages of the) MLDs are the same along the coasts and in the northeast region of our domain using the two criteria to 95 % confidence. In these regions, using the $\Delta\rho_\theta > 0.125$ criterion yields deeper MLDs. This is consistent with where salinity profiles are relatively homogeneous or compensate for the temperature change in the vertical.

The MLDs we estimate based on each of the two criteria are objectively mapped according to the method of *Le Traon* (1990), building on the work of *Bretherton et al.* (1976).

The number of grid points that had valid estimates (non-zero MLD anomalies) was largest in 2004 because that year had fewer number 852 floats than subsequent years. The number of points our objective mapping routine uses on average in a given month to describe the data are 1572 in 2002, 1605 in 2003, 1614 in 2004, 1597 in 2005, 1604 in 2006, and 1625 in 2007. We set our large scale basis function to be $1 + x + y + x^2 + y^2$, use a Poissonian covariance function, and use a decorrelation length scale of 150 kilometers.

The boundary between the seasonal and permanent thermoclines is defined to be the maximum MLD, h_m, over one year time. Here, one year is the time from when the MLD is deepest one year to when the MLD is deepest in the next year, at each horizontal grid point (e.g. Fig. 3). This can be shorter or longer than one year and this variability of time between maximum MLDs greatly influences the result. A concern is whether our results will be an artifact of better data coverage in later years. The means and standard deviations of the time-averaged MLDs and their time-averaged associated objective mapping errors calculated according to the method of *Le Traon* (1990) are shown in the top and bottom half of Figure 4 respectively. Because the spatial variance from objective mapping is constant, on the order of $10,000$ m^2, the errors are relatively small.

2.6. Parcel Tracking

Following the method of *Qiu and Huang* (1995), fluid parcels are tracked from a given initial position and time until they are obducted or run into the coast, with time steps of seven days. We track the parcel within the upper 1000 meters, and within the domain of $27 - 53^o$N and $78 - 32^o$W. The parcels are placed on a 2^o latitude by 2^o longitude by 100 meters depth grid system and tracked for each horizontal and vertical grid point. The geostrophic velocities of these water parcels are calculated subject to the vertical shear at each of these grid points. The purposes of this $2^o \times 2^o \times 100$ m grid are to: (1) resolve the vertical shear in the geostrophic flow and (2) start following water parcels from each of these grid points.

To track the parcels, a fourth-order Runge-Kutta integration was used. The numerical

time intergrations have been performed with Matlab's `ode45` (fourth-order Runge-Kutta) routine at a relative tolerance of 1%. The velocities were integrated along the trajectory of each water parcel, $u_{tr} = (u_g + u_e)/(111200 \times cos(\pi\lambda/180))$, $v_{tr} = (v_g + v_e)/111200$, and

$$w_{tr} = \begin{cases} w_e z/\delta_e + \frac{\beta}{f}\int_{-z}^{0} v_g dz` & \text{if } 0 > z > \delta_e \\ w_e + \frac{\beta}{f}\int_{-z}^{0} v_g dz` & \text{if } \delta_e > z \end{cases}$$

where λ is degrees latitude, $\delta_e = 40$ meters is the Ekman layer depth (below which u_e and v_e are 0), 111200 is the conversion factor from m/s to degrees/s, f is the Coriolis parameter allowed to vary with latitude as $sin(\pi\lambda/180)$, and β is the latitudinal derivative of f. Finally, we assume that flows just below the mixed layer are geostrophic.

We find the depths at which water columns cross h_m to find the thickness of each water parcel that gets transferred to or from the thermocline over τ, the amount of time it takes for the mixed layer to be deepest from one year to the next. Here, τ is the interval of time between releases of water parcels. A subducted (Fig. 5, top) or obducted (Fig. 5, bottom) water parcel is defined by its top and bottom. For subducted parcels, the bottom is the maximum MLD in its first year of being tracked and the top is determined by tracking the parcel. Likewise, for obducted parcels, the top is the maximum MLD in its first year of being tracked and the bottom is determined by tracking the parcel. We interpolate from a $2^o \times 2^o \times 100$ m grid onto a $1/2^o \times 1/2^o \times 20$ m grid to find the top of subducted parcels and the bottom for obducted parcels. The 20 m vertical resolution comes from our approximate error estimates in regions where ventilation is predicted to be non-zero. We have performed the same calculation with a 10 meter resolution and obtained results that are different by at most 10 m/yr, less than our error. We assume that water parcels that go outside of our model domain neither subduct if they are above the MLD nor obduct if they are below the MLD when this occurs.

2.7. Parcel Identities

Water parcel properties (temperature, salinity, etc.) are constant below the mixed layer and only change in the mixed layer. A parcel's properties, once in the permanent thermocline,

are identical to those when and where they subduct in our Lagrangian trajectory calculation so a parcel's properties are set once out of the mixed layer. Due to mixing at the surface, if a parcel comes back into the mixed layer, its properties are no longer assumed to be constant.

The waters that are EDW: (1) have temperatures between 17 and 19^oC, (2) are West of 40^oW and North of 25^oN, and (3) have a vertical temperature gradient $dT/dz < 0.006^o$C/m. *Kwon and Riser* (2004) impose (2) onto their region to calculate EDW volume. This makes at most a negligible 1% difference in volume given the two other properties of EDW. We estimate that the equivalent criterion of (3) in terms of potential vorticity, fN^2, for Brunt-Väisälä frequency $N^2 = -g/\rho(\partial\rho/\partial z)$, Coriolis parameter f, and $g = 9.81$ m/s^2 to be $|fN^2| < 1 \times 10^{-7}$ m^{-1} s^{-1}.

We calculate the vertical thickness of EDW and multiply by the area of a grid cell at each grid point to find the volume of EDW in a given month from objectively mapped thicknesses of Argo and WOCE/ACCE temperature data. This objective mapping procedure is the same as the one for the MLDs. We calculate EDW ventilation rates by using the objectively mapped temperatures from Argo and WOCE/ACCE data to identify the EDW as we track it. We do not use WOA data substitutions here because this reduces the interannual variability in the record. By tracking how much EDW enters the permanent thermocline each year, we can infer the mean annual EDW subduction rates. We do the same with EDW exiting the permanent thermocline to get the mean annual EDW obduction rates. The EDW ventilation rates are dependent upon the aforementioned mixing assumption of our model, but the EDW volume is not since it is calculated directly from data.

2.8. Error

Using an estimated variance, σ_h^2 on the order of $10,000$ m^2 for the MLDs, we may find an upper bound on the error in ventilation rate between two consecutive years. To do this, we set $(\Delta h_{err})/\tau = e_m$. Here, $(\Delta h_{err})^2 = \varepsilon_{m,0}^2 + \varepsilon_{m,1}^2$ is the sum of squared MLD errors for two consecutive years . Both $\varepsilon_{m,0}^2$ and $\varepsilon_{m,1}^2$ are computed by multiplying the associated errors from

objective mapping in percent of variance by σ_h^2. We may also estimate the ventilation rates using the lateral induction term in the *Qiu and Huang* (1995) formulation (9) with $(\Delta h_m)/\tau$.

The spatial distribution of $(\Delta h_{err})/\tau$ is similar to that of ε_m in Figure 4 but patchier. The errors are largest around 60^oW and 37.5^oW in the south and off the coast of Newfoundland. By multiplying each $(\Delta h_{err})/\tau$ and $(\Delta h_m)/\tau$ ('analytical' estimates tabulated in Table 3) by the area of a grid cell at each grid cell point and summing all of the grid points where ventilation is non-zero, we may get volume transport estimates for error and ventilation. We find that the volume transport error estimates can be as large as 50 % of our volume transport ventilation estimates.

3. Results

3.1. Ventilation Analysis

By taking advantage of new data sets, we are able to make new estimates for the quantities needed to estimate the ventilation of the thermocline in the North Atlantic. The ageostrophic currents are small in most places relative to the geostrophic ones (right-hand panel of Fig. 1). The first-order corrected ageostrophic currents only get up to 15.8 % of the geostrophic currents at any given place or time and almost never get above 10 %. The greatest geostrophic current contributions to the Ekman transports come from terms with derivatives in the geostrophic flow (e.g. $U_e \partial u_g/\partial x$). The contribution from the derivatives in the Ekman transports are negligible, both by scaling arguments and direct calculation, especially outside of the Gulf Stream.

Accounting fully for the geostrophic currents numerically, w_e is noticeably different calculating w_e directly from the wind (Fig. 6). The advection of Ekman velocities by geostrophic currents decrease w_e by 20 % where the Gulf Stream makes its sharpest turns (consistent with our ageostrophic velocities being largest there). The advection of Ekman velocities by geostrophic currents increase w_e by about a 10 % elsewhere. Comparing our w_e

with *Xie* (2004), who also used QuikSCAT winds, we see similar structure and magnitude, whereas w_e of *Qiu and Huang* (1995) is only half as big in the Gulf Stream. There is less pumping south of the Gulf Stream, in the Sargasso Sea, and less suction north of the Sargasso Sea than in *Xie* (2004).

Parcels travel at most five degrees latitudinally but may travel as many as thirty-five degrees longitudinally in a year. The means and standard deviations of longitudinal and latitudinal distances water parcels travel each year in our model are given in Table 2. Lateral induction, $(\Delta h_m)/\tau$, dominates both subduction and obduction away from the coast, contributing a few hundreds of meters per year while vertical transport contributes at most 75 m/yr in the *Qiu and Huang* (1995) formulation (9). However, vertical transport via w_e becomes quite significant close to the coasts.

With shear in weekly currents and monthly MLDs for individual years from 2002 to 2005, our ventilation rate estimates are shown in Fig. 7. This may be compared to our use of the *Qiu and Huang* (1995) formulation with associated errors (Table 3). Using the *Qiu and Huang* (1995) formulation, the errors are much less than ventilation rate estimates everywhere except the coast of Newfoundland and two southern regions of our domain. Because of these errors, the estimated magnitudes of obducted water parcels from along the coast of Newfoundland are questionable.

By taking the monthly average of the Argo-derived MLDs over 2002-2006, annual average of the currents with shear over 1999-2006, and annual average of the vertical velocities over 1999-2006, we may compute climatological ventilation rates (Fig. 8). Vertical shear in the geostrophic flow has a second-order effect on the ventilation rates. This shear may cause up to a 10 % decrease in subduction, but is not clearly out of our range of error. To see this, an average monthly MLD climatology has been constructed over 2002 to 2006 and used to calculate ventilation both with and without shear (Fig. 8, top and second to top).

Comparing the use of our $\Delta T > 0.3$ criterion (Fig. 8, top) with the $\Delta\rho_\theta > 0.125$ criterion (Fig. 8, second to bottom), we find up to a 30 % decrease in obduction using the

former because h_m is smaller in the northeast region of our domain where we estimate more obduction than subduction. The difference between total subduction and obduction is closer to zero using the $\Delta\rho_\theta > 0.125$ criterion. Comparing our estimates with and without Ekman currents (Fig. 8, top and bottom), we find up to a 15 % decrease in ventilation when $w_e = 0$.

We may also compare the climatology using the $\Delta T > 0.3$ criterion with shear to the ventilation rates we get by using the monthly Argo-derived MLDs (not averaged over 2002-2006), average of currents over 1999-2006 with shear, and average of vertical velocities over 1999-2006, and finally taking the average of these ventilation rates over 2002-2006 (Fig. 9). We find that the ventilation rates calculated using mean currents are about 5 % smaller and using mean MLDs are about 45 % smaller. The lateral induction term of (9) is mostly responsible for this (non-linear) difference in ventilation using means instead of weekly currents and monthly MLDs.

More specifically, the MLDs are not deepest in March every year (Fig. 3, bottom). For example, one year may have a deepest MLD in April and the next may have a deepest MLD in February at a given horizontal grid point, as governed by convective cooling and stratification strength. Then the ratio of Δh_m to τ may not stay constant from year to year. Here, τ is the time from when h_m is deepest one year to when h_m is deepest in the following year. The other non-linear component to ventilation rate estimation pertains to spatial distributions of currents and MLDs. The MLDs within the Gulf Stream are not as deep as they are to its south and east; as stratification is strong within the Gulf Stream, the negative buoyancy forcings are sufficiently counteracted by advected heat. The subduction rates are nonzero south and east of the Gulf Stream (Fig. 7) where the MLDs deepen most (Fig. 3, top). Their magnitudes are consistent with *Qiu and Huang* (1995).

On the other hand, the imbalance of subduction and obduction over our time series warrants further attention: as Table 4 shows, over our four years, there is a mean net subduction (subduction minus obduction) of 0.6 Sv of water with more subduction than obduction only in 2004 and 2005. A mean net subduction greater than zero would imply a shoaling of MLDs

over the time period, but this is sensitive to the domain over which this is estimated. It should be noted that if the $\Delta\rho_\theta > 0.125$ criterion were used, the MLDs in the northeast region would be deeper. There would be less subduction and more obduction. We have not tracked parcels north of 50^oN, where MLDs get deep enough to also yield more obduction that may account for the remaining discrepancy.

Lastly, we cannot estimate how long water parcels reside in the thermocline after subduction because we only have four years of data that may be tracked. However, we see that some of the parcels that reside in the thermocline for more than a year can be identified as EDW. Table 4 shows that there is a net subduction of EDW greater than zero for each of the four years while the EDW volume stays relatively stable. The EDW is not likely to travel north of 50^oN and obduct. Any EDW that travels south of 25^oN is unlikely to obduct. We may hypothesize that by properly taking mixing into account, this EDW ventilation imbalance will diminish, but we cannot test this with our model.

3.2. Density Class Analysis

The volume transport rates in our domain for σ_θ up to 28.2 kg/m^3 are in Table 4. The subducted waters come from regions South and Southeast of the Gulf Stream, while obducted waters come from regions along the Gulf Stream and closer to shore. Most of the subducted waters are slightly less dense than the obducted waters (Fig. 10), consistent with *Qiu and Huang* (1995). There is generally a right-skewed Gaussian-shaped distribution of ventilation as a function of density and a secondary peak in subduction for some years. The reason for this double peak in subduction is the local subduction minimum in the $27.2\sigma_\theta$ density class (seen barely in 2002, in 2003, and markedly in 2005), consistent with observations that there is a local minimum in oxygen concentration there (*Richards and Redfield*, 1955). It is unclear why this local minimum disappears in 2004.

Waters denser than EDW, of 27.0 kg/m^3 and above, are subducted where the ageostrophic currents are relatively large on an annual average as well as on a winter average, accelerating

the subduction process into the Gulf Stream. Waters less dense than 22.2 kg/m^3 subduct in areas where MLDs are relatively shallow and Ekman pumping is relatively strong; in particular, along the coast (Fig. 11). While subduction of the lightest waters in the slope region is consistent with the model of *Speer and Tziperman* (1992), this is the region where the errors in the Argo data are largest. The presence of water below 22.2 kg/m^3 may be an exaggeration of how light this water is. Lastly and also consistent with the model of *Speer and Tziperman* (1992), we found that Ekman pumping makes a negligible contribution to ventilation where EDW subducts (Fig. 12).

3.3. EDW Formation Charactistics

Applying the density-based criterion, $\Delta\rho_\theta > 0.125$, makes no qualitative difference in our volume estimates. The t-statistics for the differences between the mean EDW thicknesses using the density-based and temperature-based criteria over 2002 to 2006 where the EDW thicknesses are not zero do not show that there is a significant difference in the mean EDW thicknesses to 95 % confidence. Because there is no EDW along the coasts and North of 45^oN, this is consistent with where the MLD estimates are significantly different.

The density range between 25.2 and 27.8 kg/m^3 accounts for most of the ventilated waters, including newly subducted EDW in the Sargasso Sea. Most of the ventilated EDW lies within the range of σ_θ between 26.0 and 26.8 kg/m^3. This is consistent with the EDW densities of *McCartney and Talley* (1982). In 2005, the distribution of densities of ventilated EDW is wider than in previous years with a longer tail toward lower densities. This may be explained by the subduction and obduction of a wider spatial distribution of water parcels formed over a range of years.

EDW is found to form just south of the Gulf Stream. This subtropical mode water follows the North Atlantic recirculation gyre towards the south and subducts towards the edges of the recirculation gyre with a higher population of water between 17 and 19^oC during springtime (Fig. 12). We find that there is weaker stratification at the top of the thermocline where there is

EDW, consistent with the definition of EDW. There is virtually no EDW north of the Sargasso Sea because older EDW mixes and is modified by heat fluxes after entering the Gulf Stream. The rest of the water between 17 and 19^oC is of subpolar origin.

We find EDW subduction rates closer to that of *Kwon and Riser* (2004) than *Speer and Tziperman* (1992). The *Walin* (1982) formation equates the diapycnal volume flux with the difference between the air-sea buoyancy and diffusive fluxes over outcrop areas. Since the air-sea buoyancy fluxes are spatially and temporally variable, there may be substantial error in the air-sea buoyancy flux term, propagating error to the annual formation rate estimate of EDW. Additionally, neglecting mesoscale variability that contributes to diapycnal volume flux may propagate error to the annual formation rate estimate of EDW. According to our estimates as well as those of *Kwon and Riser* (2004), the *Walin* (1982) formulation appears to equate wintertime formation with annual formation.

More water between 17 and 19^oC is formed than subducts (Table 4). The differences between the EDW formation rates of *Kwon and Riser* (2004) and *Speer and Tziperman* (1992) also appear to the explained by the differences between the mean annual volume of water between 17 and 19^oC and EDW volume. Our EDW subduction and obduction rates are also tabulated in Table 4. An increase in net EDW subduction is consistent with an increase in net subduction of all waters. However, it is apparent that a net positive subduction rate of EDW does not necessarily indicate an increase in EDW volume and similarly a net positive obduction rate of EDW does not dictate a decrease in EDW volume. The missing EDW from this picture is (a) EDW that is modified in the main thermocline, (b) newly formed EDW in the mixed layer that has not obducted, and (c) EDW that is not modified after obducting.

The spatial distribution of the errors in EDW volume is the same as that of the MLDs because the same objective mapping procedure was applied to the EDW thicknesses themselves. By estimating the thickness of water between 17 and 19^oC via objectively mapped Argo temperatures, we find similar volumes to the thickness objective mapping procedure until 2005 and 2006 when the thickness objective mapping procedure yields EDW volumes

that are twice as large. The spatial distributions of EDW and seasonal variability of its volume between the order of 1×10^{14} m^3 and about 10×10^{14} m^3 are robust. Using a combination of objectively mapped temperatures from both Argo and WOA data yields EDW volumes with a depressed seasonal variation.

Subducted waters are about the same density on average as obducted waters. However, while obducted water may generally be colder than subducted water, obducted waters are generally warmer relative to their surroundings than subducted waters. Similarly, since EDW is cold relative to surrounding waters in the mixed layer, we reason that the mixed layer should be coldest in 2002, warm due to an increase in net subduction of EDW from 2002 to 2004, and cool due to a decrease in net subduction of EDW in 2005. Consistent with this, the winter (January through March average) mixed layer (potential) temperature means and standard deviations respectively for our domain are 16.3^oC and 4.76^oC (4023 data points) for 2002, 16.7^oC and 4.82^oC (4134 data points) for 2003, 16.8^oC and 5.02^oC (4010 data points) for 2004, 17.6^oC and 4.77^oC (3885 data points) for 2005, and 17.0^oC and 5.02^oC (3987 data points) for 2006.

4. Conclusions

The wind stresses are significantly dependent upon the relative velocities between the winds and the geostrophic currents. This affects the Ekman divergences by about $10 - 20$ % as well as the Sverdrup transports. Even so, vertical pumping is increasingly negligible relative to lateral induction farther away from the coast. Including a small vertical shear can make about a 10 % difference in ventilation rates, albeit within our error.

Because the ratio of Δh_m to τ is not constant, 'analytical' estimates of ventilation rates may be inaccurate. The use of climatologies in our Lagrangian trajectory method may underestimate ventilation by similar reasoning. Nevertheless, the length of our time series may also explain the underestimates of ventilation. By how much averaging MLDs matters remains uncertain but appears to be marginally larger than our error: at most 50 %. Winter mixed

layer temperatures change in concert with net (EDW) ventilation rates, suggestive that mixed layer temperature variability may be closely linked to ventilation rate variability. However, the criterion by which we calculate the MLDs may affect obduction estimates because of a difference in h_m where salinity profiles have significantly different gradients than elsewhere.

Subducted waters tend to come from south of the Gulf Stream, while obducted waters come from along the Gulf Stream. The lightest waters subduct at the coast where vertical velocities can dominate MLD variability. Water heavier than EDW is aided by the ageostrophic currents in subduction more than other waters. Both lateral induction and vertical pumping are non-negligible in the Gulf Stream. MLD variability matters most for ventilation elsewhere.

WOA data have been used in related studies (e.g. *Kwon* (2003) and *Joyce et al.* (2000)), but due to the relatively unpronounced seasonal variability in WOA data, the temporal resolution made possible by the Argo system allows us to investigate variability at higher frequencies. The importance of intra-annual variations in MLDs, for instance, must be emphasized in estimating EDW ventilation rates. These rates are greatest during the springtime when the mixed layer shallows. Some of the subducted EDW resides in the thermocline for a period longer than the length of our time series: at least 3.5 years. This warrants future investigations because the EDW residence time may play a crucial role in the heat budget and a potential NAO-EDW coupled oscillation.

5. Appendix

Starting from the momentum-balance equations for an incompressible fluid and neglecting viscosity, we have the set of coupled partial differential equations (PDEs),

$$\frac{\partial u}{\partial t} + u\frac{\partial u}{\partial x} + v\frac{\partial u}{\partial y} + w\frac{\partial u}{\partial z} - fv = \frac{1}{\rho}\frac{\partial \tau^x}{\partial z} - \frac{1}{\rho}\frac{\partial p}{\partial x} \tag{13}$$

$$\frac{\partial v}{\partial t} + u\frac{\partial v}{\partial x} + v\frac{\partial v}{\partial y} + w\frac{\partial v}{\partial z} + fu = \frac{1}{\rho}\frac{\partial \tau^y}{\partial z} - \frac{1}{\rho}\frac{\partial p}{\partial y} \tag{14}$$

where the zonal, meridional, and vertical currents are $u = u_e + u_g$, $v = v_e + v_g$, and $w = w_e$, respectively, the sums of their Ekman and geostrophic contributions. Ageostrophic currents,

which include Ekman currents, are defined to be the difference between the total currents and the geostrophic currents. Here, non-Ekman ageostrophic currents and vertical geostrophic currents are ignored. Furthermore, because we have defined the geostrophic current in terms of the gradient of the total pressure field, the pressure gradients cancel with the geostrophic currents without derivatives (*Holton*, 2004).

Now we apply the following assumptions: (a) The geostrophic currents are vertically uniform in the Ekman layer. This is reasonable if we assume the Ekman layer depth is finer than our vertical resolution. (b) The geostrophic currents obey quasi-geostrophic dynamics. That is, $\partial u_g/\partial t + u_g \partial u_g/\partial x + v_g \partial u_g/\partial y - f v_a = 0$ and $\partial v_g/\partial t + u_g \partial v_g/\partial x + v_g \partial v_g/\partial y + f u_a = 0$ to first-order. Here, 'a' denotes 'ageostrophic' but non-Ekman. This essentially assumes that Rossby number, $Ro = U/fL$, is much less than unity. The ageostrophic current terms are of order Ro compared to the geostrophic velocities. Also, the vertical velocity, w, is of the order of Ro compared to aspect ratio scaling. Thus, by vertically integrating over the Ekman layer with depth, δ_e, we get the set of coupled PDEs,

$$\begin{aligned} \frac{\partial (U_e + \delta_e u_g)}{\partial t} + \int_{-\delta_e}^{0} u_e \frac{\partial u_e}{\partial x} dz + U_e \frac{\partial u_g}{\partial x} + u_g \frac{\partial U_e}{\partial x} + \delta_e u_g \frac{\partial u_g}{\partial x} + \\ \int_{-\delta_e}^{0} v_e \frac{\partial u_e}{\partial y} dz + V_e \frac{\partial u_g}{\partial y} + v_g \frac{\partial U_e}{\partial y} + \delta_e v_g \frac{\partial u_g}{\partial y} + \int_{-\delta_e}^{0} w_e \frac{\partial u}{\partial z} dz - f V_e - f V_a &= \frac{\tau^x}{\rho} \quad (15) \\ \frac{\partial (V_e + \delta_e v_g)}{\partial t} + \int_{-\delta_e}^{0} u_e \frac{\partial v_e}{\partial x} dz + U_e \frac{\partial v_g}{\partial x} + u_g \frac{\partial V_e}{\partial x} + \delta_e u_g \frac{\partial v_g}{\partial x} + \\ \int_{-\delta_e}^{0} v_e \frac{\partial v_e}{\partial y} dz + V_e \frac{\partial v_g}{\partial y} + v_g \frac{\partial V_e}{\partial y} + \delta_e v_g \frac{\partial v_g}{\partial y} + \int_{-\delta_e}^{0} w_e \frac{\partial v}{\partial z} dz + f U_e + f U_a &= \frac{\tau^y}{\rho}. \quad (16) \end{aligned}$$

The integrated zonal Ekman currents are U_e and the intergrated meridional Ekman currents are V_e. The Ekman currents are so smooth that, in fact, all first-order derivatives of them turn out to be negligible. This may also be seen by a scaling argument. Thus, with one further assumption, that (c) terms to second order in u_e and v_e (e.g. $\int_{-\delta_e}^{0} dz u_e \partial u_e/\partial x$) are negligible, we find:

$$\begin{aligned} U_e \frac{\partial u_g}{\partial x} + u_g \frac{\partial U_e}{\partial x} + V_e \frac{\partial u_g}{\partial y} + v_g \frac{\partial U_e}{\partial y} - f V_e &= \frac{\tau^x}{\rho} \quad (17) \\ U_e \frac{\partial v_g}{\partial x} + u_g \frac{\partial V_e}{\partial x} + V_e \frac{\partial v_g}{\partial y} + v_g \frac{\partial V_e}{\partial y} + f U_e &= \frac{\tau^y}{\rho}. \quad (18) \end{aligned}$$

After introducing τ_{damp} to iteratively find a numerical solution, we get Equations 7 and 8.

We may, alternatively, solve for the Ekman transports, U_e and V_e, explicitly if we assume (a), (b), (c), and make further assumptions about the strengths of the Ekman and geostrophic currents and their derivatives in space with respect to one another: If (d) $(\partial u_e/\partial x)/(\partial u_g/\partial x) \ll 1$, (e) $u_g/u_e \ll 1$ (similarly for derivatives in y and for the meridional currents), and (f) products of derivatives in any currents are negligible, then we get,

$$U_e \approx \frac{1}{\rho}\left(\frac{\tau^x \frac{\partial v_g}{\partial y}}{(f(f+\frac{\partial v_g}{\partial x}-\frac{\partial u_g}{\partial y}))}+\frac{\tau^y}{(f+\frac{\partial v_g}{\partial x})}\right) \tag{19}$$

$$V_e \approx \frac{1}{\rho}\left(\frac{\tau^y \frac{\partial u_g}{\partial x}}{(f(f+\frac{\partial v_g}{\partial x}-\frac{\partial u_g}{\partial y}))}-\frac{\tau^x}{(f-\frac{\partial u_g}{\partial y})}\right). \tag{20}$$

From these analytical results, we can find $w_e = \partial U_e/\partial x + \partial V_e/\partial y$ to get,

$$w_e \approx \frac{1}{\rho}\frac{1}{(f+\frac{\partial v_g}{\partial x}-\frac{\partial u_g}{\partial y})}\Big(\frac{\partial \tau^y}{\partial x}-\frac{\partial \tau^x}{\partial y}-\frac{\beta}{f}\tau^x-\frac{\beta}{(f+\frac{\partial v_g}{\partial x}-\frac{\partial u_g}{\partial y})}$$
$$\times((\tau^y-\tau^x)(\frac{\partial v_g}{\partial x}-\frac{\partial u_g}{\partial y})+2(f(\tau^y-\tau^x)-\tau^x(\frac{\partial v_g}{\partial x}-\frac{\partial v_g}{\partial y})+\tau^y(\frac{\partial u_g}{\partial x}-\frac{\partial u_g}{\partial y})))). \tag{21}$$

It is assumption (e) that fails almost everywhere, but this is our first guess in numerically solving for the Ekman currents. Note that a negative value for w_e represents water transport from the Ekman layer down to the mixed layer because of how we have defined this quantity. A positive Ekman suction is a positive w_e and a positive Ekman pumping is a negative w_e.

Acknowledgments.

The authors would like to acknowledge Suzanne Dickinson for preparing the QuikSCAT gridded wind speed field, and Li Ren for some of the Argo data.

QuikSCAT winds are available at:
http://podaac-www.jpl.nasa.gov/cgi-bin/dcatalog/fam_summary.pl?ovw+qscat.

Aviso SSHs are available at:
http://www.aviso.oceanobs.com/html/donnees/produits/hauteurs/global/msla_uk.html.

Argo temperatures and salinities are available at:
http://www.usgodae.org/ftp/outgoing/argo/geo/atlantic_ocean.

WOA temperature and salinity climatologies are available at:
http://www.cdc.noaa.gov/cdc/data.nodc.woa94.html.

References

Bretherton, F. P., R. E. Davis, and C. B. Fandry, 1976, A technique for objective analysis and design of oceanographic experiments applied to MODE-73. *Deep-Sea Res.*, **23**, 559–582.

Curry, R. G. and M. S. McCartney, 2001, Ocean Gyre Circulation Changes Associated with the North Atlantic Oscillation, *J. Phys. Ocean.*, **31**, 3374–3400.

Dong, S., K. Kelly, Heat Budget in the Gulf Stream Region, 2004: The Importance of Heat Storage and Advection, *J. Phys. Ocean.*, **34**(05), 1214–1231.

Dong, S., S. L. Hautala, K. A. Kelly, 2007: Interannual Variations in Upper Ocean Heat Content and Heat Transport Convergence in the Western North Atlantic, *J. Phys. Oceanogr.*, **37**(11), 2682–2697.

Harrison, D. E., 1989; On climatological monthly mean wind stress and wind stress curl fields over the World Ocean. *J. Climate*, **2**, 57–70.

Hellerman, S., M. Rosenstein, 1983: Normal monthly wind stress over the world ocean with error estimates, *J. Phys. Ocean.*, **13**, 1093–1104.

Holton, J. R., 2004; An Introduction to Dynamic Meteorology. *Academic Press*, 4th Edition.

Kelly, K. A., S. Dickinson, and Z.-J. Yu, 1999: NSCAT tropical wind stress maps: Implications for improving ocean modeling, *J. Geophys. Res.*, **104**(11), 11,291–11,310.

Kwon, Y.-O., 2003: Observation of General Circulation and Water Mass Variability in the North Atlantic Subtropical Mode Water Region. PhD Dissertation, *University of Washington*, Seattle.

Kwon, Y.-O., S. Riser, 2004: North Atlantic Subtropical Mode Water: A history of ocean-atmosphere interaction 1961-2000, *Geophys. Res. Lett.*, **31**(10), L19307.

Iselin, C. O. .D., 1939: The influence of vertical and lateral turbulence on the characteristics of the waters at mid-depths, *Trans. Amer. Geophys. Union*, **28**(20), 1–26.

Joyce, T. M., C. Deser, M. A. Spall, 2000: The Relation between Decadal Variability of Subtropical Mode Water and the North Atlantic Oscillation, *J. Climate*, **13**, 2550–2569.

Le Traon, P. Y., 1990, A Method for Optimal Analysis of Fields With Spatially Variable Mean. *J. Geophys. Res.*, **93**(8), 13,543–13,547.

Marshall, J. C., A. J. G. Nurser, R. G. Williams, 1993: Inferring the Subduction Rate and Period over the North Atlantic, *J. Phys. Ocean.*, **23**(07), 1315–1329.

McCartney, M. S. and L. D. Talley, 1982: The subpolar mode water of the North Atlantic Ocean, *J. Phys. Oceanogr.*, **12**, 1169–1188.

Nurser, A. J. G., R. Marsh, J. C. Marshall, 1999: Diagnosing water mass formation from air-sea fluxes and surface mixing, *J. Phys. Ocean.*, **29**, 1468–1487.

Palter, J. B., M. S. Lozie, R. T. Barber, 2005: The effect of advection on the nutrient reservoir in the North Atlantic subtropical gyre. *Nature*, **437**, 687–692.

Qiu, B., R. X. Huang, 1995: Ventilation of the North Atlantic and North Pacific: Subduction Versus Obduction, *J. Phys. Ocean.*, **25**(10), 2374–2390.

Richards, F. A., A. C. Redfield, 1955: Oxygen-density relationships in the western North Atlantic Ocean. *Deep-Sea Res.*, **2**, 182–189.

Seager, R., Y. Kushnir, M. Visbeck, N. Naik, J. Miller, G. Krahmann, H. Cullen, 2000: Causes of Atlantic Ocean climate variability between 1958 and 1998. *J. Climate*, **13**, 2845–2862.

Singh, S., and K. A. Kelly, 1997: Monthly maps of sea surface height in the North Atlantic and zonal indices for the Gulf Stream using TOPEX/Poseidon altimeter data. Technical report, WHOI.

Snedecor, George W. and W. G. Cochran, 1989: *Statistical Methods, Eighth Edition*, Iowa State University Press.

Speer, K., E. Tziperman, 1992: Rates of Water Mass Formation in the North Atlantic Ocean, Speer, K., *J. Phys. Ocean.*, **25**(01), 93–104.

Stommel, H., 1995: Determination of water mass properties of water pumped down from the Ekman layer to the geostrophic flow below, Stommel, H., *Collected Works of Henry Stommel*, II-207,II-211,Vol. II,Chap. 1.

Walin, G., 1982: On the relation between sea-surface heat flow and thermal circulation in the ocean. *Tellus*, **34**, 187–195.

Williams, R. G., Ocean subduction, 2001: *Science*, **109**, 10,1982–1983.

Worthington, L., 1959: The 18^o water in the Sargasso Sea. *Deep-Sea Res.*, **5**, 297–305.

Xie, S.-P., 2004: Satellite observations of cool ocean-atmosphere interaction, Xie, S.-P., *Bull. Amer. Meteor. Soc.*, **85**(02),195–208.

School of Oceanography, Box 355351, University of Washington, Seattle, WA 98195.
trossd@u.washington.edu

Received _____

Figure Captions

Figure 1. Average of the geostrophic and ageostrophic (as estimated from the first-order quasi-geostrophic equations described in the Appendix) currents from Aviso in the Gulf Stream region over 1999 to 2006.

Figure 2. Locations of non-852 Argo floats that reported data in the month of March from 2002 to 2005.

Figure 3. The MLDs in March (top) and the month numbers (e.g. March $= 3$) when the MLDs reach a maximum in late winter/early spring of 2004 (left) and 2007 (right). These are the years with the most and least spatial coverage by non-WMO 852 Argo floats from when WMO 852 Argo floats errors were introduced.

Figure 4. Top-left: Mean of the MLDs over 2002 to 2007 in meters. Top-right: Standard deviation of the MLDs over 2002 to 2007 in meters. Bottom-left: Mean of the associated objective mapping errors over 2002 to 2007 in meters. Bottom-right: Standard deviation of the associated objective mapping errors over 2002 to 2007 in meters.

Figure 5. The atmosphere, surface Ekman layer, mixed layer, seasonal thermocline, and permanent thermocline are shown to represent an idealized cross-section across a strong density gradient. The gray parallelograms are approximate representations of the water columns that either subduct or obduct. Here, h_m is the boundary between the seasonal and permanent thermocline. In the top case, the water column subducts and stays in the permanent thermocline. In the bottom case, the water column obducts. The dashed arrow indicates time evolution, the interval it takes for the MLD to be deepest from one year to the next. For simplicity, h_m is the same in each year.

Figure 6. The average of Ekman pumping [in m/yr] in the Gulf Stream and Sargasso Sea regions, including currents (solved numerically) over 1999 to 2006 (top) and the difference between the average of w_e [in m/yr] including currents and that without currents in the same region over the same time period (bottom).

Figure 7. The mean annual subduction [in m/yr] (left) and obduction [in m/yr] (right) rates for 2002-2003 (top), 2003-2004 (second to top), 2004-2005 (second to bottom), and 2005-2006 (bottom) using monthly-varying MLDs and weekly-varying currents with shear. The corresponding volume transport [in Sv] is in the lower right-hand corner box of each plot.

Figure 8. The mean annual subduction [in m/yr] (left) and obduction [in m/yr] (right) rates using 1999-2006 average currents and a climatology of 2002-2005 average monthly-varying MLDs. The top corresponds to using the $\Delta T > 0.3$ criterion with vertical current shear. The second to top corresponds to using the $\Delta T > 0.3$ criterion with no vertical current shear. The second to bottom corresponds to using the $\Delta\rho_\theta > 0.125$ criterion with vertical current shear. The bottom corresponds to using the $\Delta T > 0.3$ criterion and vertical shear, but no Ekman currents ($w_e = 0$). The corresponding volume transport in and out of the permanent thermocline [in Sv] is in the lower right-hand corner box of each plot.

Figure 9. The mean subduction [in m/yr] (left) and obduction [in m/yr] (right) rates over 2002-2006 using mean velocities and mean MLDs (top), using mean velocities and estimated monthly MLDs (middle), and using estimated weekly velocities and estimated monthly MLDs (bottom), all with shear. The corresponding volume transport in and out of the permanent thermocline [in Sv] is in the lower right-hand corner box of each plot.

Figure 10. Volume transports [in Sv] categorized into subduction (gray positive bars), EDW subduction (black positive bars), obduction (gray negative bars), and EDW obduction (black negative bars), broken into intervals of 0.2 kg/m^3 for (a) 2002, (b) 2003, (c) 2004, and (d) 2005.

Figure 11. Locations of where at anomalously large subduction rates of heavy water, 27.0 kg/m^3 and above, [x] and light water, 22.0 kg/m^3 and below, [o] occurs for (a) 2002, (b) 2003, (c) 2004, and (d) 2005.

Figure 12. Thickness of waters between 17 and 19^oC [in meters] in springtime (April-June) with locations where greater than average subduction rates of EDW occur in our domain [x] in (a) 2002, (b) 2003, (c) 2004, and (d) 2005.

Tables

Table 1. The data we used in our calculations

Quantity	Winds	SSH	MLD, σ_θ, EDW, shear	shear
Source	QuikSCAT	Aviso	Argo, WOCE/ACCE	WOA
Dates	Jan 02-Aug 06	Jan 02-Aug 06	Jan 02-Jun 07	pre-1994
Frequency	daily	weekly	every 10 days	monthly

Table 2. Means and standard deviations (std) of the longitudinal and latitudinal distances water parcels travel in a given year through our model

Distances	2002	2003	2004	2005
mean of longitudinal distance [^{o}]	6.24	6.34	6.40	6.19
std of longitudinal distance [^{o}]	6.87	7.07	7.55	7.48
mean of latitudinal distance [^{o}]	1.11	0.989	0.963	1.07
std of latitudinal distance [^{o}]	1.48	1.24	1.37	1.32

Table 3. Spatial mean and standard deviation (std) of subduction and obduction, and root mean square (rms) error: 'analytical' ($(\Delta h)/\tau$ from *Qiu and Huang* (1995)) versus modeled ['-' is insufficient data]

estimation	2002	2003	2004	2005	2006
Analytical rms error [m/yr]	74.7	57.6	41.2	48.3	44.1
Analytical subduction mean [m/yr]	45.1	58.7	67.3	46.5	46.3
Analytical subduction std [m/yr]	50.5	68.5	69.8	40.2	51.6
Modeled subduction mean [m/yr]	51.8	57.5	52.8	54.9	-
Modeled subduction std [m/yr]	59.3	57.5	49.9	56.3	-
Modeled obduction mean [m/yr]	64.6	63.9	49.6	47.1	-
Modeled obduction std [m/yr]	79.9	73.2	57.9	53.9	-

Table 4. Ventilation and EDW rates and EDW volume from 2002 to 2006 [‘-‘ is insufficient data]

mean annual quantity	2002	2003	2004	2005	2006
$17-19^{o}$C water volume [10^{14} m^3]	4.44	8.78	10.3	13.5	12.8
$17-19^{o}$C water subduction [Sv]	3.72	8.17	6.10	6.20	-
$17-19^{o}$C water obduction [Sv]	1.30	1.70	2.03	2.30	-
EDW volume [10^{14} m^3]	1.58	1.63	1.69	1.35	1.89
EDW subduction [Sv]	0.80	1.86	1.74	3.65	-
EDW obduction [Sv]	0.43	0.72	1.00	1.12	-
Subduction [Sv]	17.4	19.0	18.1	18.2	-
Obduction [Sv]	20.4	20.5	15.5	13.9	-

Figures

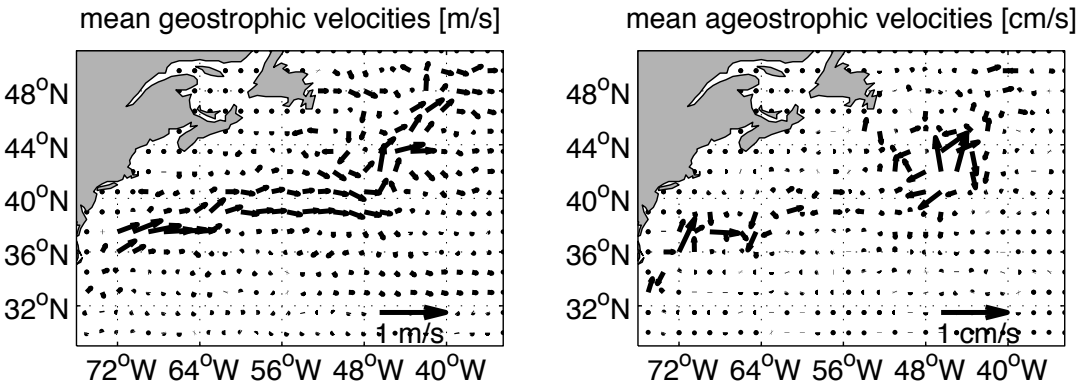

.

Figure 1. Average of the geostrophic and ageostrophic (as estimated from the first-order quasi-geostrophic equations described in the Appendix) currents from Aviso in the Gulf Stream region over 1999 to 2006.

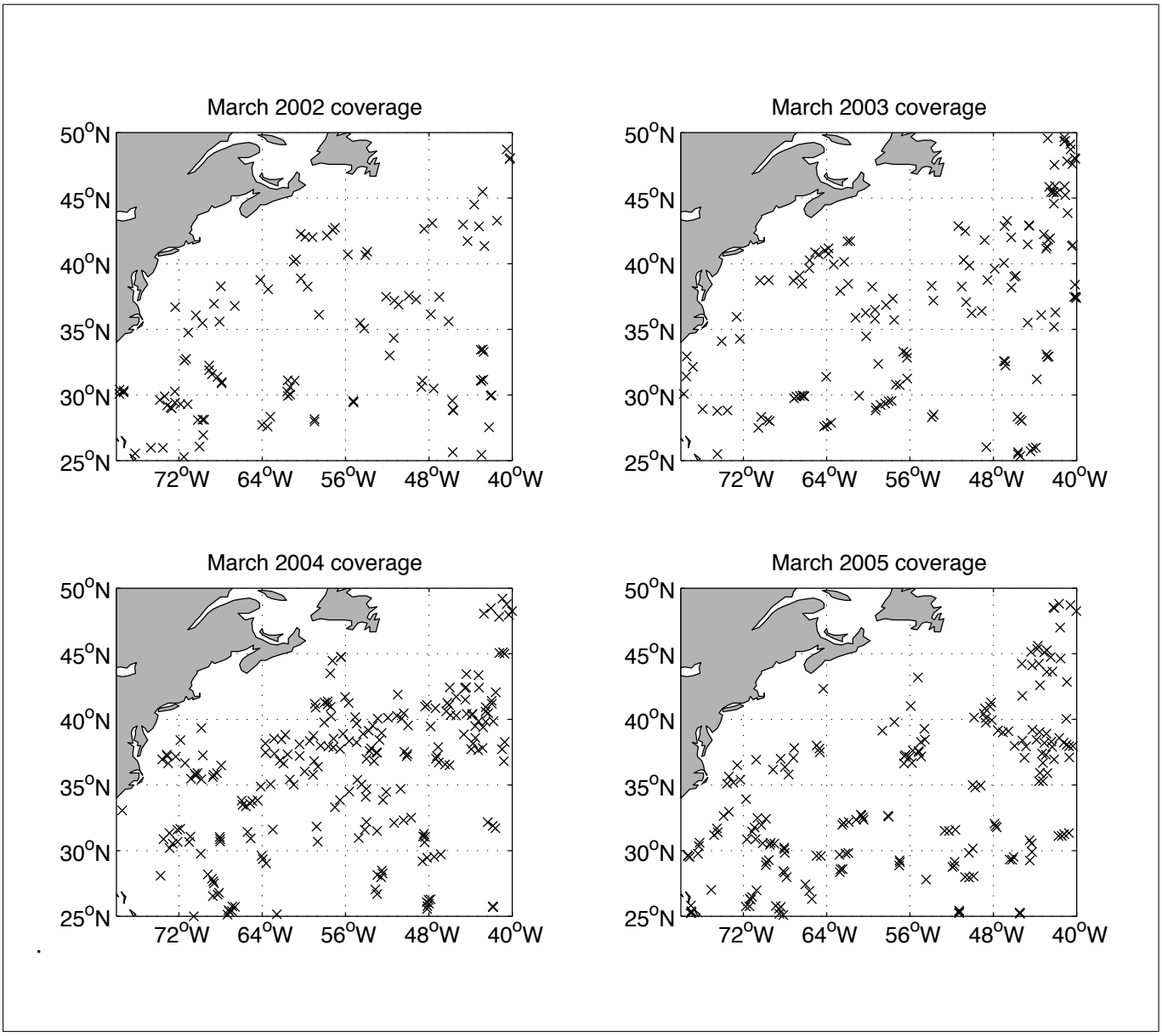

Figure 2. Locations of non-852 Argo floats that reported data in the month of March from 2002 to 2005.

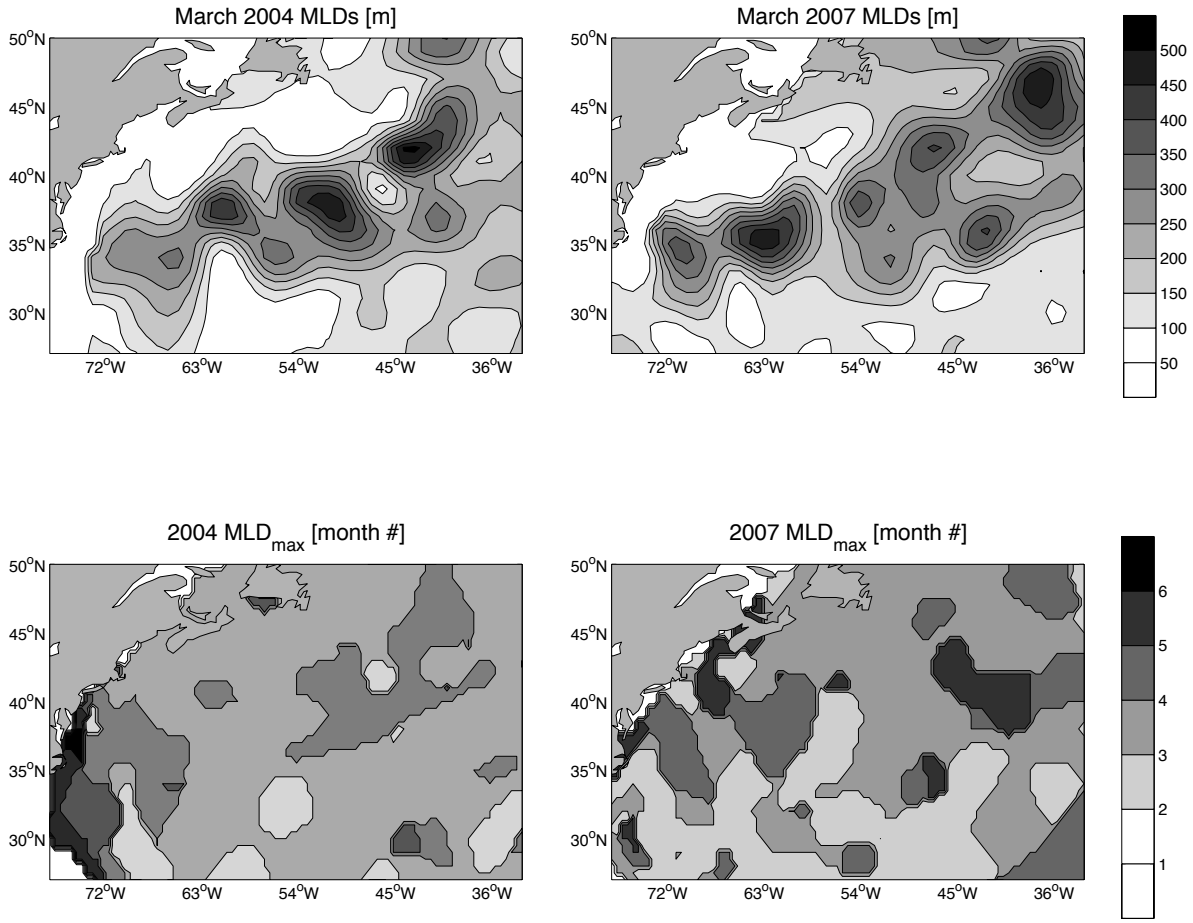

Figure 3. The MLDs in March (top) and the month numbers (e.g. March $= 3$) when the MLDs reach a maximum in late winter/early spring of 2004 (left) and 2007 (right). These are the years with the most and least spatial coverage by non-WMO 852 Argo floats from when WMO 852 Argo floats errors were introduced.

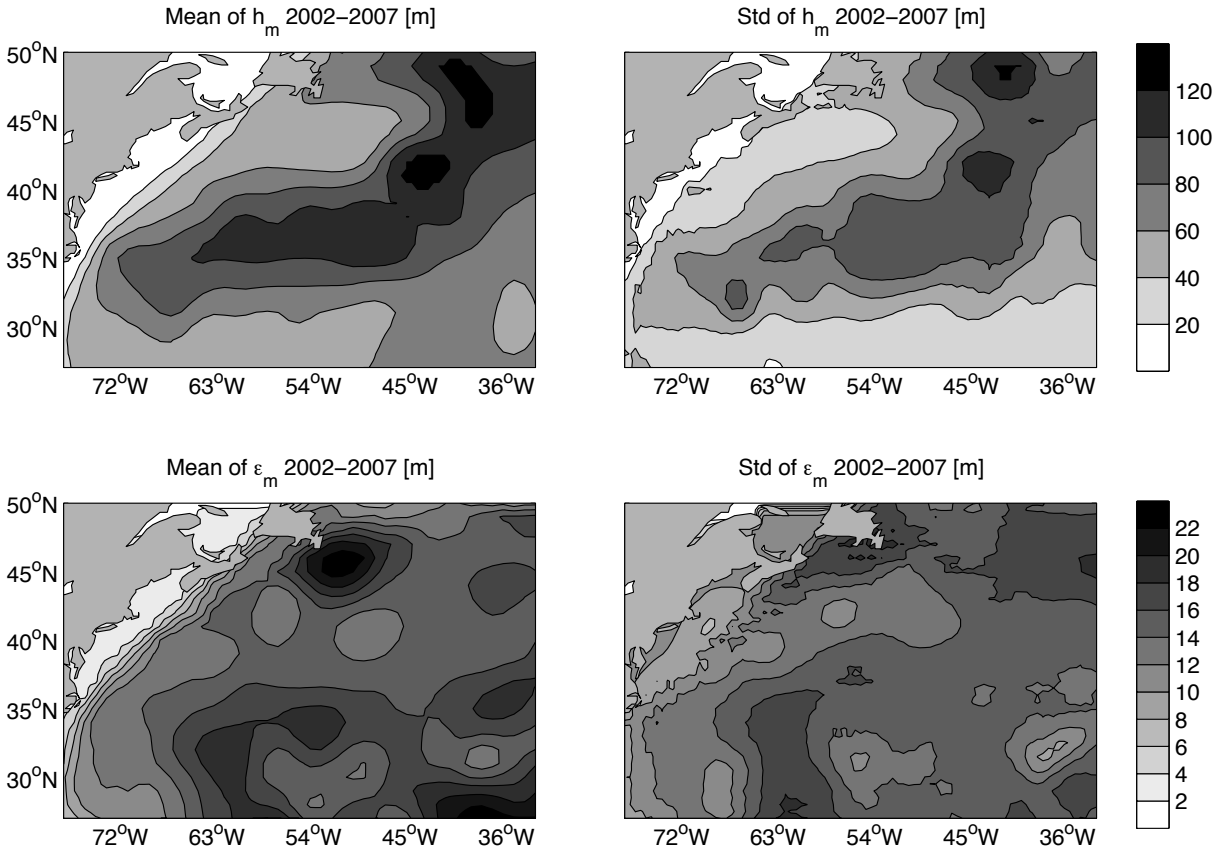

Figure 4. Top-left: Mean of the MLDs over 2002 to 2007 in meters. Top-right: Standard deviation of the MLDs over 2002 to 2007 in meters. Bottom-left: Mean of the associated objective mapping errors over 2002 to 2007 in meters. Bottom-right: Standard deviation of the associated objective mapping errors over 2002 to 2007 in meters.

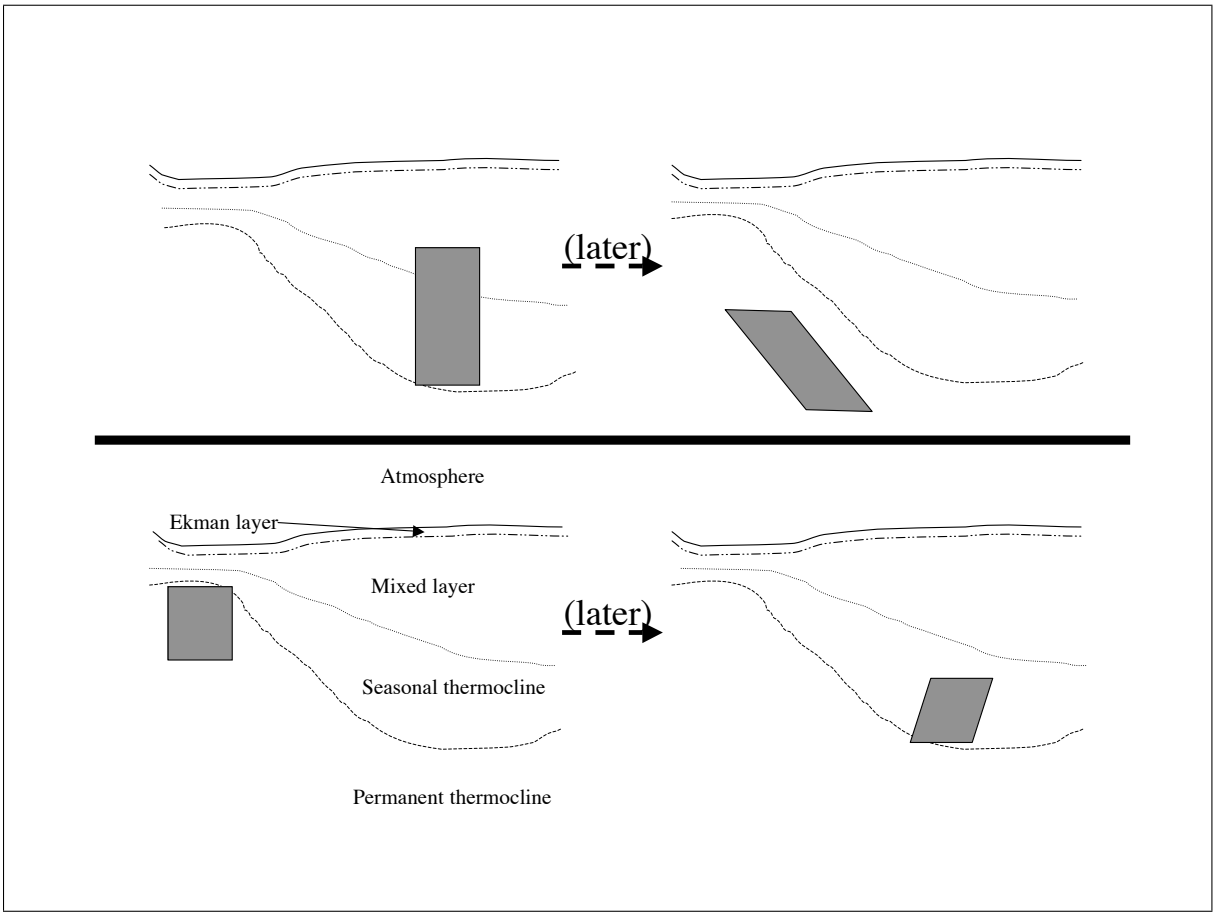

Figure 5. The atmosphere, surface Ekman layer, mixed layer, seasonal thermocline, and permanent thermocline are shown to represent an idealized cross-section across a strong density gradient. The gray parallelograms are approximate representations of the water columns that either subduct or obduct. Here, h_m is the boundary between the seasonal and permanent thermocline. In the top case, the water column subducts and stays in the permanent thermocline. In the bottom case, the water column obducts. The dashed arrow indicates time evolution, the interval it takes for the MLD to be deepest from one year to the next. For simplicity, h_m is the same in each year.

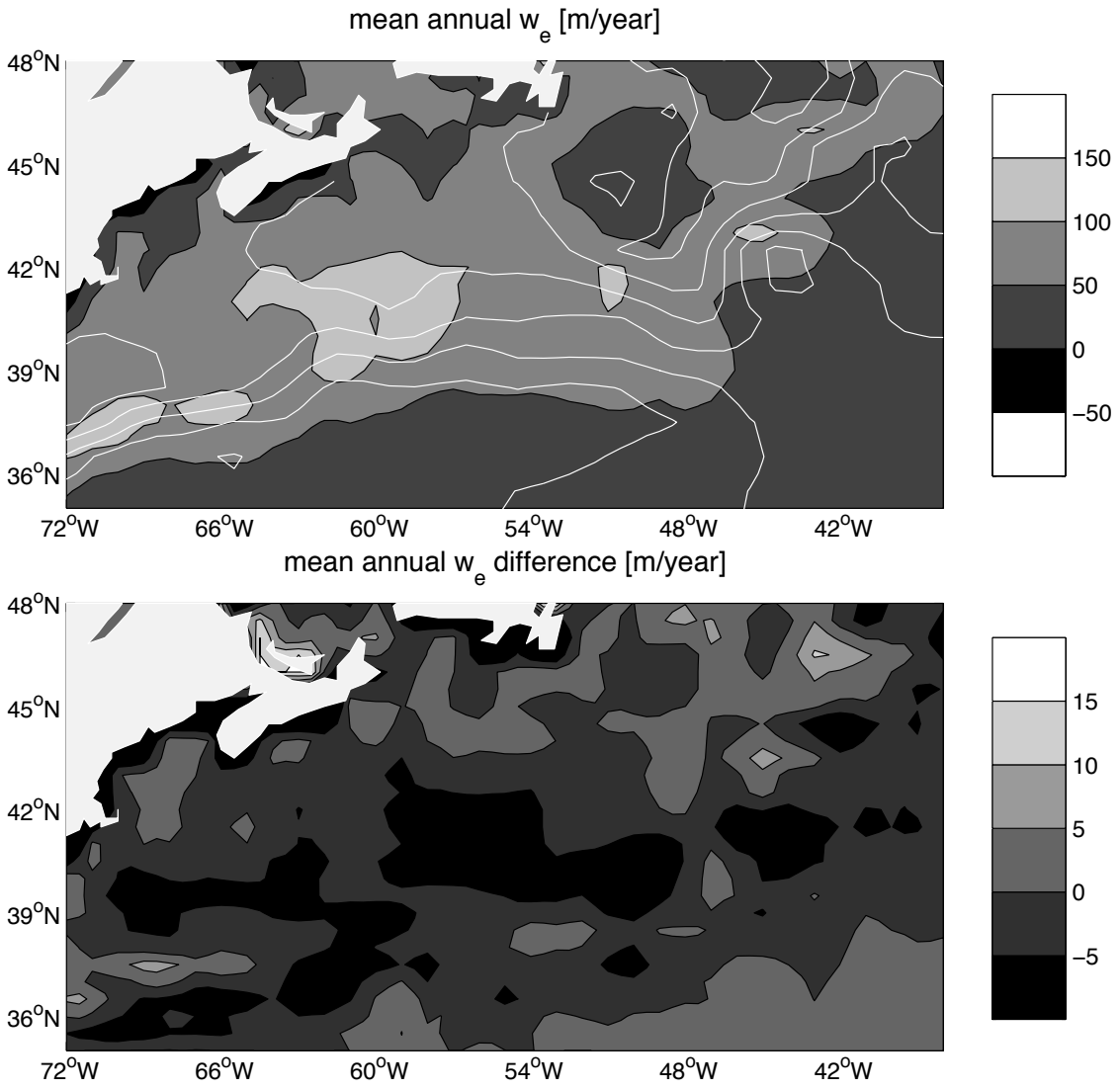

Figure 6. The average of Ekman pumping [in m/yr] in the Gulf Stream and Sargasso Sea regions, including currents (solved numerically) over 1999 to 2006 (top) and the difference between the average of w_e [in m/yr] including currents and that without currents in the same region over the same time period (bottom).

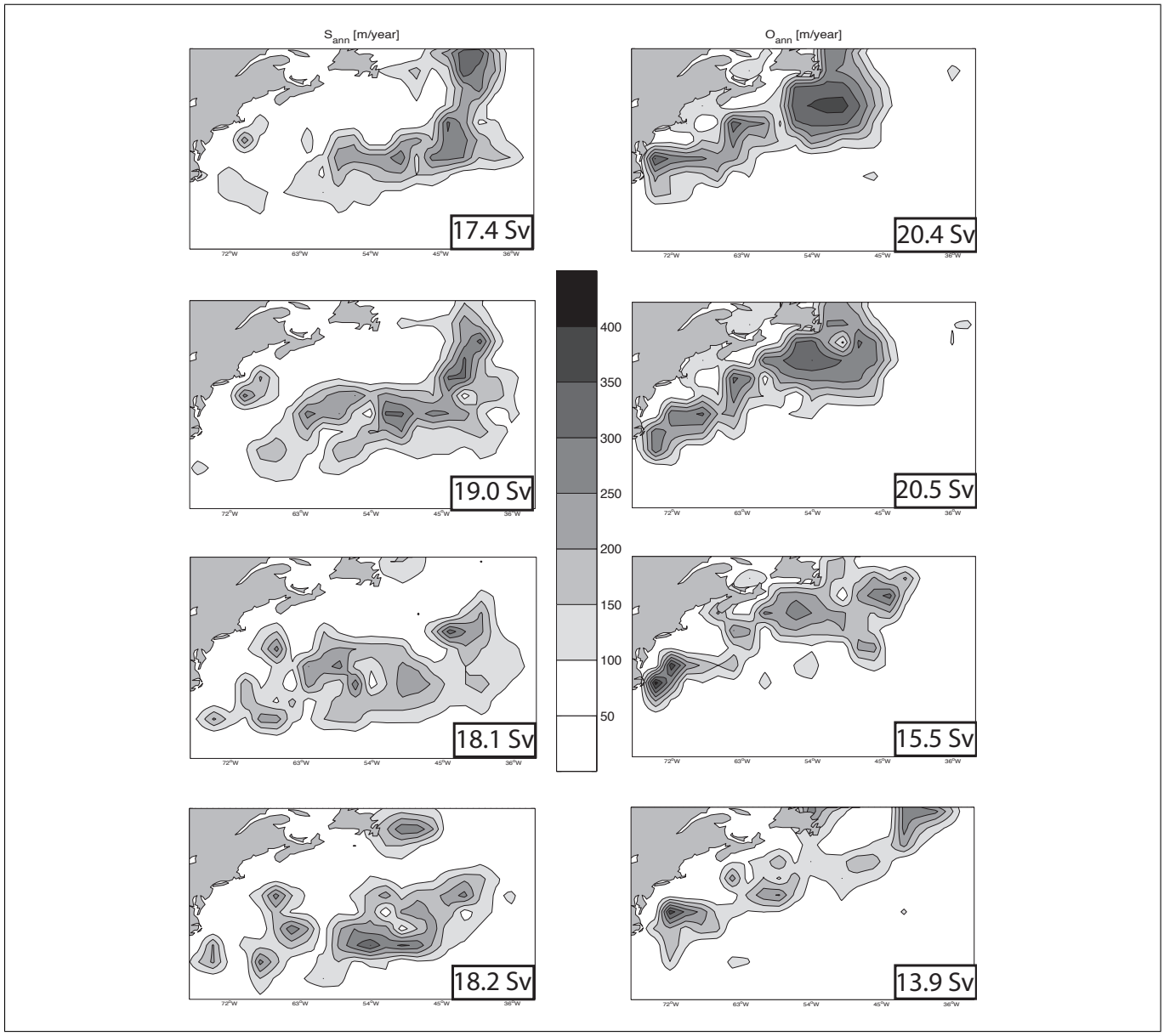

Figure 7. The mean annual subduction [in m/yr] (left) and obduction [in m/yr] (right) rates for 2002-2003 (top), 2003-2004 (second to top), 2004-2005 (second to bottom), and 2005-2006 (bottom) using monthly-varying MLDs and weekly-varying currents with shear. The corresponding volume transport [in Sv] is in the lower right-hand corner box of each plot.

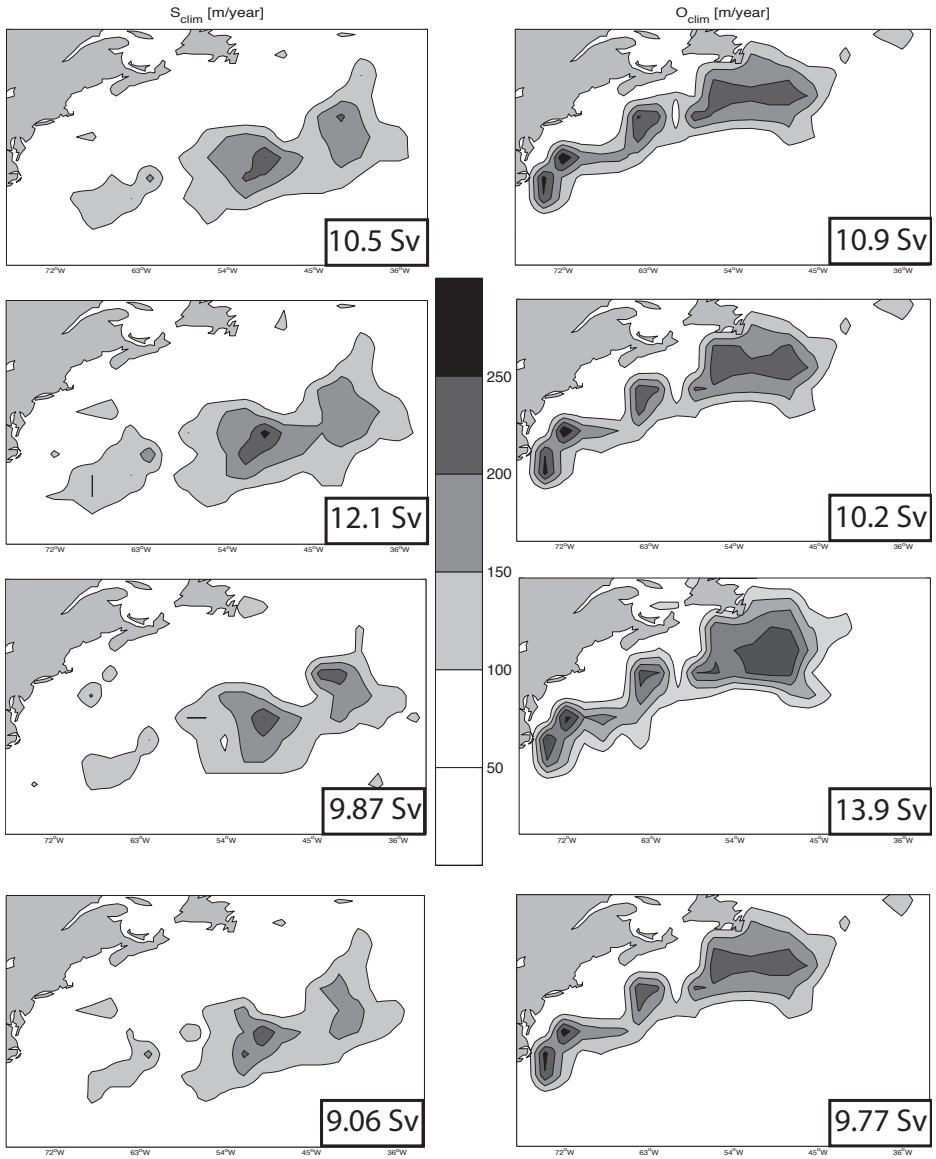

Figure 8. The mean annual subduction [in m/yr] (left) and obduction [in m/yr] (right) rates using 1999-2006 average currents and a climatology of 2002-2005 average monthly-varying MLDs. The top corresponds to using the $\Delta T > 0.3$ criterion with vertical current shear. The second to top corresponds to using the $\Delta T > 0.3$ criterion with no vertical current shear. The second to bottom corresponds to using the $\Delta\rho_\theta > 0.125$ criterion with vertical current shear. The bottom corresponds to using the $\Delta T > 0.3$ criterion and vertical shear, but no Ekman currents ($w_e = 0$). The corresponding volume transport in and out of the permanent thermocline [in Sv] is in the lower right-hand corner box of each plot.

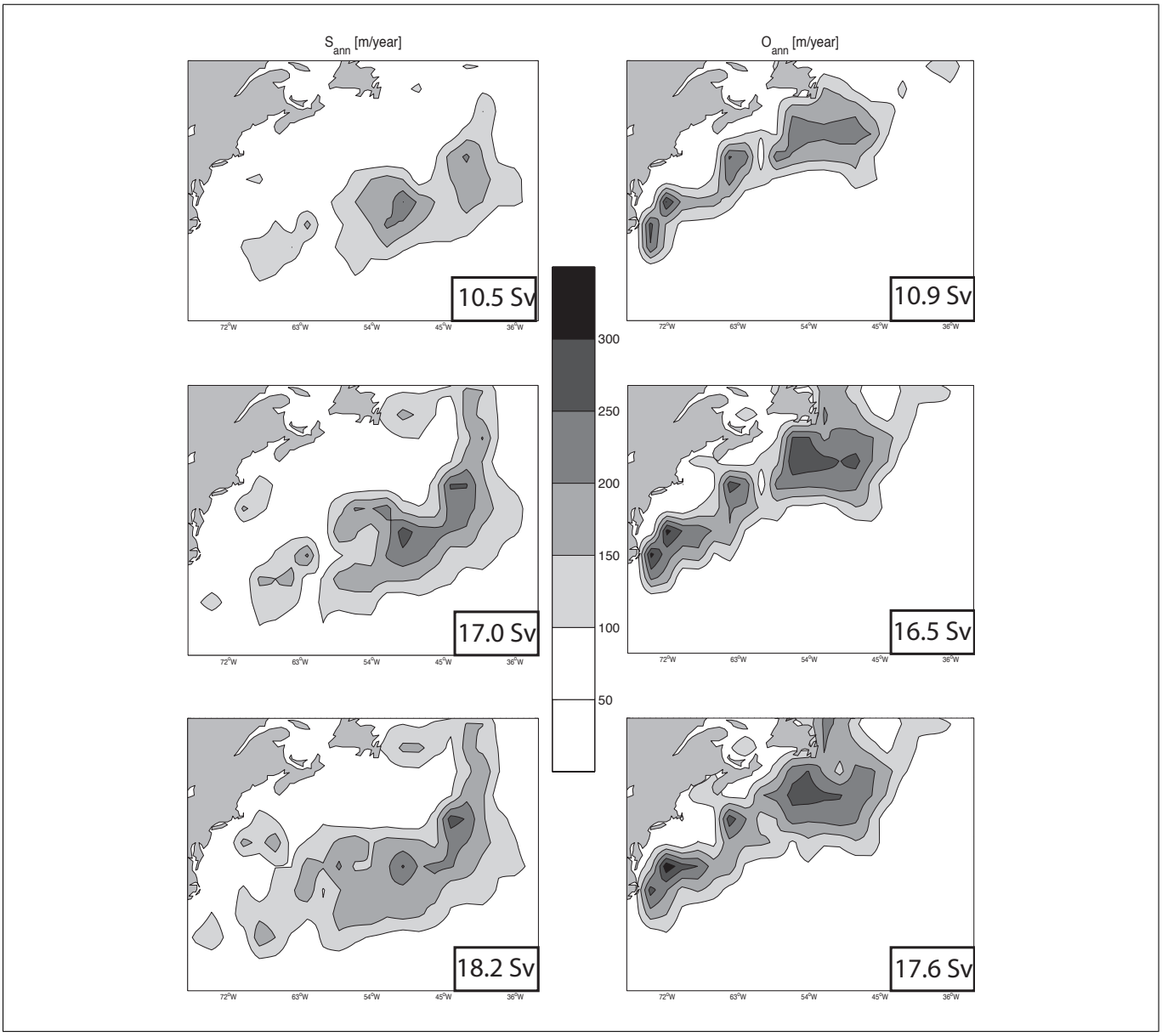

Figure 9. The mean subduction [in m/yr] (left) and obduction [in m/yr] (right) rates over 2002-2006 using mean velocities and mean MLDs (top), using mean velocities and estimated monthly MLDs (middle), and using estimated weekly velocities and estimated monthly MLDs (bottom), all with shear. The corresponding volume transport in and out of the permanent thermocline [in Sv] is in the lower right-hand corner box of each plot.

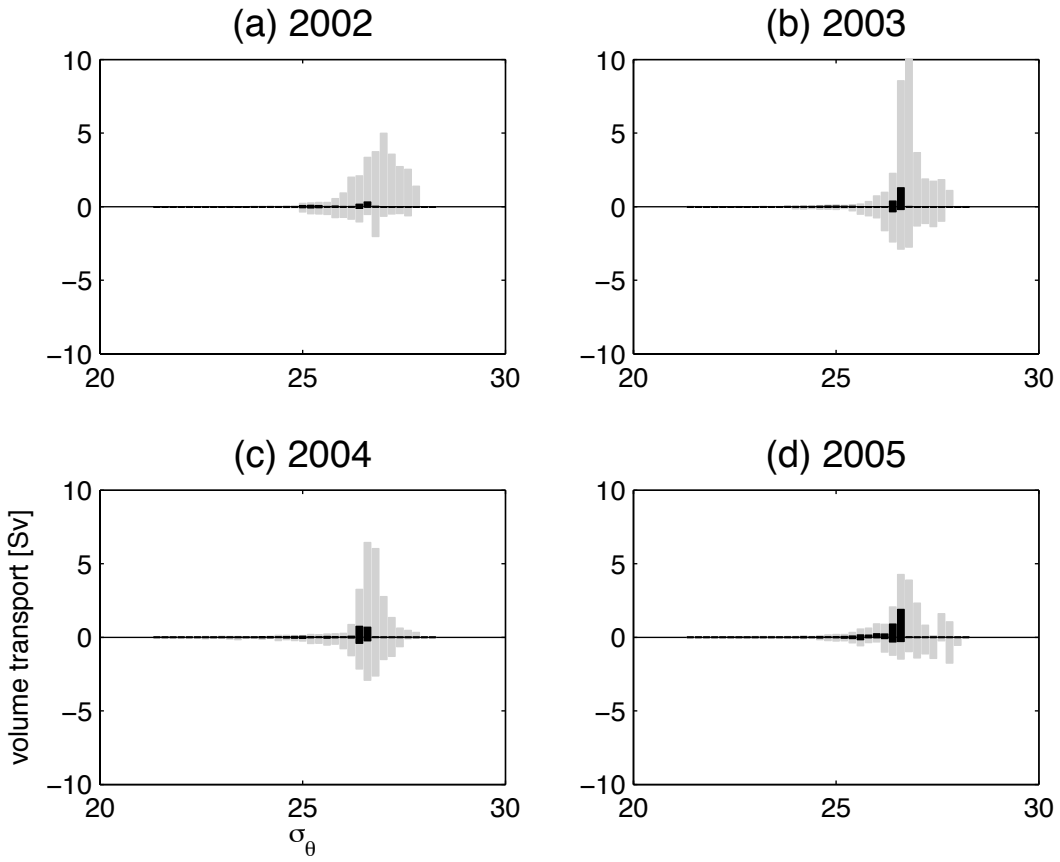

Figure 10. Volume transports [in Sv] categorized into subduction (gray positive bars), EDW subduction (black positive bars), obduction (gray negative bars), and EDW obduction (black negative bars), broken into intervals of 0.2 kg/m^3 for (a) 2002, (b) 2003, (c) 2004, and (d) 2005.

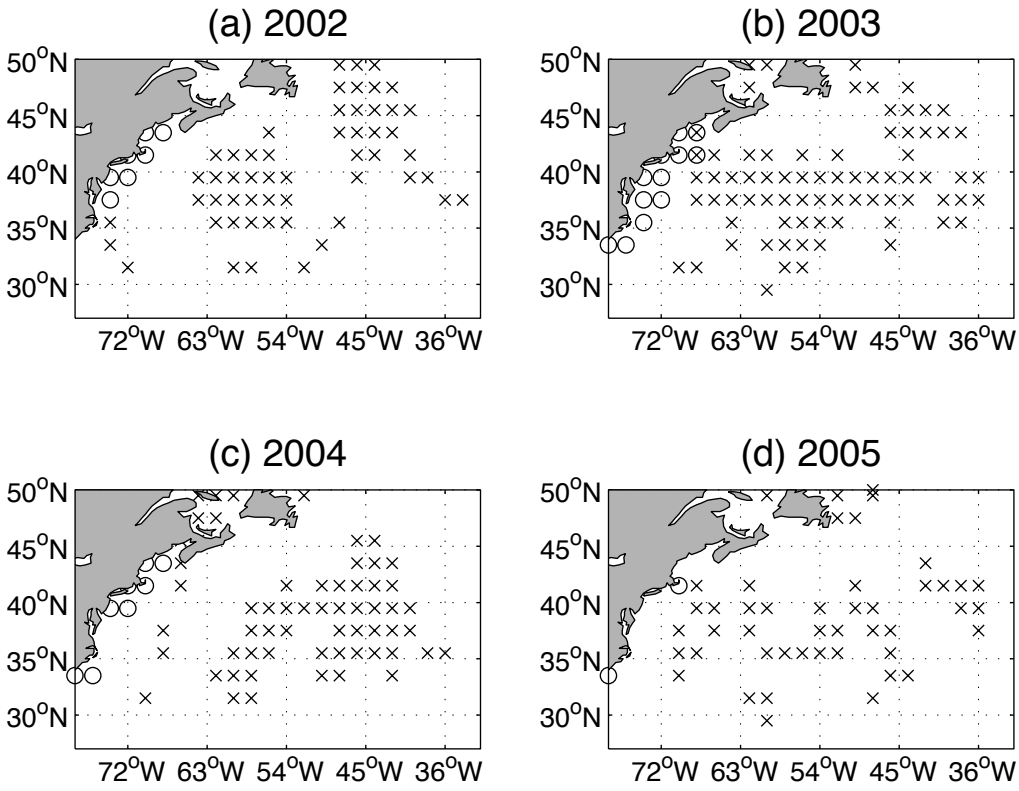

Figure 11. Locations of where at anomalously large subduction rates of heavy water, 27.0 kg/m^3 and above, [x] and light water, 22.0 kg/m^3 and below, [o] occurs for (a) 2002, (b) 2003, (c) 2004, and (d) 2005.

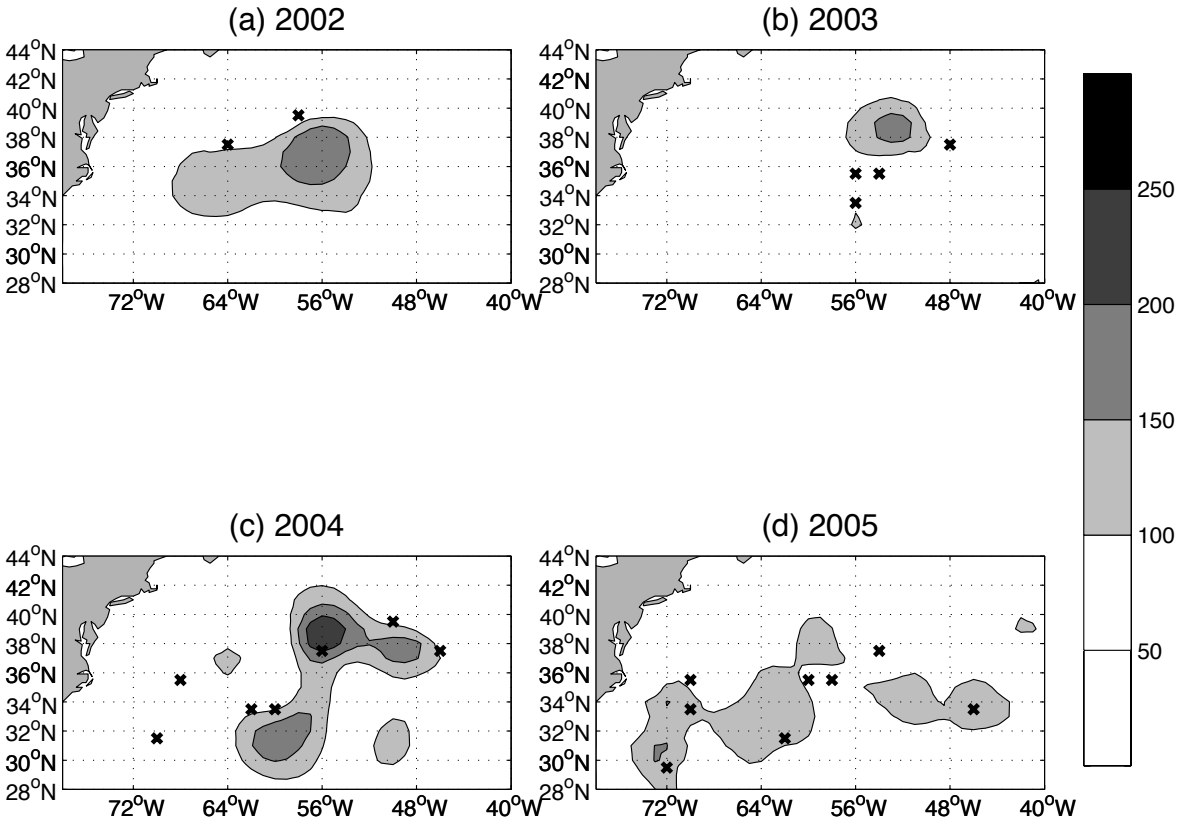

Figure 12. Thickness of waters between 17 and 19^{o}C [in meters] in springtime (April-June) with locations where greater than average subduction rates of EDW occur in our domain [x] in (a) 2002, (b) 2003, (c) 2004, and (d) 2005.